Available online at www.sciencedirect.com
ScienceDirect
Journal of Solid State Chemistry 180 (2007) 2926–2932
JOURNAL OF SOLID STATE CHEMISTRY
www.elsevier.com/locate/jssc

Crystal structure and electronic properties of the new compounds, $U_6Fe_{16}Si_7$ and its interstitial carbide $U_6Fe_{16}Si_7C$

D. Berthebaud[a], O. Tougait[a,*], M. Potel[a], E.B. Lopes[b], A.P. Gonçalves[b], H. Noël[a]

[a]*Laboratoire de Chimie du Solide et de Matériaux. UMR CNRS 6226, Université de Rennes 1, 263 Avenue de Général Leclerc, 35042 Rennes, France*
[b]*Departamento de Química, Instituto Tecnológico e Nuclear/CFMC-UL, P-2686-953 Sacavém, Portugal*

Received 1 June 2007; received in revised form 17 July 2007; accepted 29 July 2007
Available online 22 August 2007

Abstract

The new compounds $U_6Fe_{16}Si_7$ and $U_6Fe_{16}Si_7C$ were prepared by arc-melting and subsequent annealing at 1500 °C. Single-crystal X-ray diffraction showed that they crystallize in the cubic space group $Fm\bar{3}m$ (No. 225), with unit-cell parameters at room temperature $a = 11.7206(5)$ Å for $U_6Fe_{16}Si_7$ and $a = 11.7814(2)$ Å for $U_6Fe_{16}Si_7C$. Their crystal structures correspond to ordered variants of the Th_6Mn_{23} type. $U_6Fe_{16}Si_7$ adopts the $Mg_6Cu_{16}Si_7$ structure type, whereas $U_6Fe_{16}Si_7C$ crystallizes with a novel "filled" quaternary variant. The inserted carbon is located in octahedral cages formed by six U atoms, with U–U interatomic distances of 3.509(1) Å. Insertion of carbon in the structure of $U_6Fe_{16}Si_7$ has a direct influence on the U–Fe and Fe–Fe interatomic distances. The electronic properties of both compounds were investigated by means of DC susceptibility, electrical resistivity and thermopower. $U_6Fe_{16}Si_7$ is a Pauli paramagnet. Its electrical resistivity and thermopower point out that it cannot be classified as a simple metal. The magnetic susceptibility of $U_6Fe_{16}Si_7C$ is best described over the temperature range 100–300 K by using a modified Curie–Weiss law with an effective magnetic moment of 2.3(2) μ_B/U, a paramagnetic Weiss temperature, $\theta_p = 57(2)$ K and a temperature-independent term $\chi_0 = 0.057(1)$ emu/mol. Both the electrical resistivity and thermopower reveal metallic behavior.

Keywords: Actinide; Uranium; Iron; Heavy Fermion; Magnetic susceptibility; Electrical resistivity; Thermopower

1. Introduction

Uranium-based compounds exhibit a great variety of physical phenomena, such as itinerant (Pauli) or localized (Curie–Weiss) paramagnetism, spin-glass or long-range magnetic order, Kondo behavior, heavy fermion and superconductivity. It is considered that these electronic features are mainly related to the degree of hybridization of the 5*f* electrons with the conduction and/or other valence electrons. In this respect, the intermetallic systems combining U and Fe have to be considered of considerable importance due to the high degree of delocalization of the U 5*f* electrons that directly hybridize with the Fe 3*d* electrons [1]. As a consequence, the magnetic moments borne by the U atoms are small and often negligible [2]. However, the influence of the U sublattice is substantial, as evidenced by the comparison of the magnetic properties of the isostructural compounds obtained with magnetic as well as non-magnetic rare-earth elements [3,4]. In U-based compounds, the value of the Curie temperature is significantly different, the magnetic anisotropy is strong and the magnetic moments carried by the iron atoms are considerably reduced up to the cancellation, in some cases. In this respect, the ternary phases of the U–Fe–Si system can be considered as typical examples.

This ternary system, which has been extensively studied, comprises ten intermediate phases. Beside $UFe_{10}Si_2$ [5], $U_2Fe_{17-x}Si_x$ ($3.3 < x < 4.5$) [6] and UFe_5Si_3 [7] which order ferromagnetically at high temperature, but with low values of the magnetic moments on iron atoms, $U_{1.2}Fe_4Si_{9.7}$ [8] is the only compound showing Curie–Weiss behavior. Its effective magnetic moment of 2.4 μ_B/U is significantly reduced from the free ion values of 3.62 and 3.58 μ_B/U for U^{3+} and U^{4+}, respectively, and also suggests that the local magnetic moment carried by the Fe atoms is negligible. All

*Corresponding author. Fax: +33 2 23 23 67 99.
E-mail address: tougait@univ-rennes1.fr (O. Tougait).

0022-4596/$ - see front matter © 2007 Elsevier Inc. All rights reserved.
doi:10.1016/j.jssc.2007.07.030

other reported phases, U_2FeSi_3 [9], UFeSi [10], U_2Fe_3Si [11], $U_3Fe_2Si_7$ [12], $U_2Fe_3Si_5$ [13] and UFe_2Si_2 [14] exhibit magnetic behaviors that are governed by itinerant electrons. To probe the influence of the U concentration on the magnetic moment carried by iron atoms, a detailed investigation of the Fe-rich corner of the U–Fe–Si ternary phase diagram, as well as the measurement of the electronic properties of the intermediate phases have been undertaken [7,15]. During this experimental work, the new compound $U_6Fe_{16}Si_7$ has been found. It crystallizes in a ternary ordered variant of the Th_6Mn_{23} type of structure, which is able to accommodate small atoms in octahedral holes to give cage-filled compounds, as already encountered for $Sc_{11}Ir_4$ [16] and $Zr_6Zn_{23}Si$ [17] or the *G* phases [18]. Therefore, the synthesis of the interstitial carbide $U_6Fe_{16}Si_7C$ was attempted and successfully obtained, its magnetic and transport properties were measured to also provide data to our investigation. In this paper, we present the details of the synthesis, the crystal structure refinements and measurements of the magnetization, electrical resistivity and thermoelectrical power of the new uranium and iron intermetallics, $U_6Fe_{16}Si_7$ and $U_6Fe_{16}Si_7C$.

2. Experimental

Starting materials for the synthesis of $U_6Fe_{16}Si_7$ and $U_6Fe_{16}Si_7C$ were uranium turnings (nuclear grade), iron pieces (Strem, 5N), silicon (Strem, 6N) and carbon rod (Strem, 5N). For the preparation of $U_6Fe_{16}Si_7C$, the C was first combined with U in uranium monocarbide. Calculated amounts of the components were melted under low pressure of argon, in an arc-furnace. In order to ensure a good homogeneity, the buttons were flipped and re-melted two times. To promote crystallization, heat treatments at high temperature were undertaken. Some samples were introduced in alumina crucible, before being sealed into molybdenum crucibles that were previously outgased. Both $U_6Fe_{16}Si_7$ and $U_6Fe_{16}Si_7C$ were heated at a rate of 100 °C/h up to 1500 °C, held there for 10 h and then cooled at 50 °C/h to 1000 °C, at which temperature, the furnace was turn off and allowed to cool down to room temperature. Single crystals were mechanically isolated from crushed as-cast and heat-treated ingots.

Scanning electron microscopy and energy-dispersive spectroscopy (SEM–EDS) were performed on pieces of each sample embedded in resin and polished using SiC paper and diamond paste down to 1 μm. A thin layer of gold was deposited on their surfaces before metallographic analyses. The compositional contrast among the various phases was revealed by means of a backscattered electron detector on a 6400-JSM scanning electron microscope and chemical analyses were obtained with an Oxford Link Isis energy-dispersive spectrometer. Additional corrections were superimposed to the internal ZAF corrections through the use of stoichiometric external standards, U_3Si_2 and FeSi.

X-ray powder diffraction patterns were recorded using an Inel CPS 120 diffractometer working with a $K\alpha_1$ Co radiation. Single-crystal X-ray diffraction experiments were performed on a Nonius Kappa CCD diffractometer. The unit-cell parameters, orientation matrix as well as the crystal quality were derived from 10 frames recorded at $\chi = 0$ using a scan of 1° in ϕ. The complete strategy to fill more than a hemisphere was automatically calculated with the use of the program COLLECT [19]. Data reduction and reflection indexing were performed with the program DENZO of the Kappa CCD software package [19]. The scaling and merging of redundant measurements of the different data sets as well as the cell refinement was performed using DENZO. Semi-empirical absorption corrections were made with the use of the programs MULTISCAN [20]. Structure models were determined by direct methods using SIR-97 [21]. All structures refinements and Fourier syntheses were made with the help of SHELXL-97 [22].

The electrical resistivity was measured in a closed-cycle refrigerator in the 18–300 K temperature range using the four-probe AC method. The thermoelectric power was measured relative to gold by a slow AC technique (10^{-2} Hz), with a thermal gradient of 1 K, in a home-made apparatus similar to the one previously described by Chaikin and Kwak [23].

DC magnetic measurements were carried out using a Quantum Design MPMS-5 SQUID magnetometer. Data were collected in the temperature range 2–300 K with applied fields of 5 kOe. The magnetization was measured at 5 K in increasing and decreasing magnetic fields up to 50 kOe.

3. Results

3.1. Phase formation

The existence of the new compound $U_6Fe_{16}Si_7$ was revealed during the systematic investigation of the U–Fe–Si ternary phase diagram. Several samples with initial atomic ratios in the vicinity of U:Fe:Si of 20:55:25 were prepared. Both metallographic observations and EDS analyses carried out on as-cast and heat-treated samples show the formation of a new ternary phase which appears isopointal to the $Mg_6Cu_{16}Si_7$ type on the X-ray powder patterns. Methodical microprobe analyses confirm that no solid solubility around the ideal composition could be detected, indicating that $U_6Fe_{16}Si_7$ is a point compound.

3.2. Crystal structure refinements

Three crystals selected from samples of different starting compositions and with or without heat treatment were investigated by X-ray diffraction techniques. The main crystallographic details are gathered in Table 1. Single crystal labeled A, was isolated from an as-cast sample having as initial composition $U_6Fe_{16}Si_7$. Refinements of the

Table 1
Crystal data and structure refinements of $U_6Fe_{16}Si_7$ (A), $U_6Fe_{16}Si_7C_{0.91}$ (B) and $U_6Fe_{16}Si_7C$ (C)

Crystal label	A	B	C
Empirical formula	$U_6Fe_{16}Si_7$	$U_6Fe_{16}Si_7C_{0.80(1)}$	$U_6Fe_{16}Si_7C$
Formula weight (g/mol)	2518.44	2528.0	2530.44
Crystal system, space group	Cubic, $Fm\bar{3}m$ (no. 225)		
Unit cell dimensions (Å)	11.7206(5)	11.7814(2)	11.7786(2)
Volume (Å^3)	1610.09(2)	1635.3(1)	1634.1(1)
Z, Calculated density (g/cm^3)	4, 10.39	4, 10.27	4, 10.29
Absorption coefficient (cm^{-1})	741	733	734
Crystal color	Black	Black	Black
Crystal size (mm^3)	$0.15 \times 0.1 \times 0.1$	$0.3 \times 0.15 \times 0.2$	$0.3 \times 0.15 \times 0.2$
Theta range for data collection (deg.)	3–40	3–45.1	3–42
Limiting indices	$-21 \leqslant h \leqslant 21$	$-23 \leqslant h \leqslant 21$	$-22 \leqslant h \leqslant 14$
	$-20 \leqslant k \leqslant 21$	$-22 \leqslant k \leqslant 23$	$-21 \leqslant k \leqslant 22$
	$-21 \leqslant l \leqslant 12$	$-23 \leqslant l \leqslant 19$	$-20 \leqslant 1 \leqslant 22$
Reflections collected/unique	8644/304	12026/399	9562/344
R(int)	0.16	0.080	0.11
Absorption correction	Semi-empirical (MULTISCAN [10])		
Refined parameters	15	17	16
Goodness-of-fit on F^2	1.25	1.09	1.11
wR_2 ($I > 2\sigma(I)$])	0.109	0.069	0.050
R [$I > 2\sigma(I)$]	0.047	0.027	0.021
Extinction coefficient	0.00002(1)	0.00040(4)	0.00039(3)
Largest difference peak and hole (e/Å^3)	6.13/−2.87	2.79/−2.79	2.49/−1.91

$R(F) = \Sigma||F_o| - |F_c||/|F_c|$, $wR_2 = \left[\Sigma w\left(F_o^2 - F_c^2\right)^2 / wF_o^4\right]^{1/4}$, where $w^{-1} = [\sigma^2(F_o^2) + 7.27P]$, $P = [\max(F_o^2, 0) + 2F_c^2]/3$.

structure converged to a structural model with a distribution of atoms similar to that reported for the $Mg_6Cu_{16}Si_7$ type, with a cubic space group $Fm\bar{3}m$ and a lattice parameter at room temperature $a = 11.7206(5)$ Å. The residual factors are slightly larger that those of crystals B and C, but compare well with the residual values obtained from the refinements on single crystals of the G phase recently published [18]. The maximum residual electron density of about 6 electrons per Å^3, which is located on the 4*b* Wyckoff site, is usual for U-based compounds having such a large unit-cell volume [24,25]. This low value precludes any occupancy of this position by carbon or oxygen atoms, which would require electron density of about 16 or 20 electrons per Å^3 (see Refs. [17,26] and below, crystal B).

Single crystal B, was chosen from a sample $U_6Fe_{16}Si_7$ heat treated at 1500 °C. The atomic positions of $U_6Fe_{16}Si_7$ obtained from crystal A, were taken as an initial model for the crystallographic refinement. At the first stage of the refinement, a positive peak in the Fourier synthesis of about 22 electrons per Å^3 was revealed on the 4*b* Wyckoff site. The coordination polyhedron around this position is composed of 6 U atoms in an octahedral motif, with intersite distance of about 2.5 Å. Such small interatomic distance disqualifies the occupancy of this crystallographic position by iron or silicon. Moreover, the EDS analyses did not show any detectable solid solubility around the ideal composition. They also did not show any impurity from elements having atomic numbers above 10. Therefore, only small atoms can be considered as interstitial elements. Regarding that oxygen and/or carbon are the main impurity elements found in metal elements or introduced during handlings, they were successively tested in the structural model. Subsequent refinements including anisotropic displacement parameters for all atoms yield low values of the residual factors and a flat Fourier map. In the final refinements, the occupancy of the interstitial atom located on the 4*b* site was allowed to freely vary, giving the chemical formulae $U_6Fe_{16}Si_7O_{0.53(1)}$ or $U_6Fe_{16}Si_7C_{0.80(1)}$. Chemical analyses using SEM–EDS techniques did not allow to properly ascribe the nature of this light interstitial element present with an atomic ratio of less than 3 at%.

Single crystal C was selected from a sample with nominal composition $U_6Fe_{16}Si_7C$ heat treated at 1500 °C. The initial structure calculations were carried out with U, Fe and Si on crystallographic positions of the $Mg_6Cu_{16}Si_7$ type. Fourier synthesis showed at the 4*b* Wyckoff site, a significant electron density of about 24 electrons per Å^3, which was assigned to a carbon atom. In subsequent refinements the occupancy of the 4*b* site was allowed to vary, yielding a partial occupation of 0.96(1), which was therefore constrained to one. Final refinements rapidly converged to the low residual factors gathered in Table 1 and yielded a featureless Fourier map. Another indirect evidence of the insertion of small atoms in the octahedral voids, is the significant enlargement of the unit-cell parameter a, which increase from $a = 11.7206(5)$ Å in the unfilled model (crystal A) to a value close to 11.78 Å, for the filled structures (crystals B and C). Tables 2 and 3 report the positional and equivalent isotropic displacement parameters, and a selection of the interatomic distances,

Table 2
Atomic parameters of $U_6Fe_{16}Si_7$(A) and $U_6Fe_{16}Si_7C$ (C)

Atom	Wyckoff position	x	y	z	$U_6Fe_{16}Si_7$ (A)		$U_6Fe_{16}Si_7C$ (C)	
					x	U_{eq} (Å^2)	x	U_{eq} (Å^2)
U	24*e*	x	0	0	0.2859(1)	0.017(1)	0.2894(1)	0.012(1)
Fe(1)	32*f*	x	x	x	0.1212(1)	0.017(1)	0.1222(1)	0.013(1)
Fe(2)	32*f*	x	x	x	0.3276(1)	0.017(1)	0.3255(1)	0.013(1)
Si(1)	24*d*	0	1/4	1/4		0.016(1)		0.014(1)
Si(2)	4*a*	0	0	0		0.012(1)		0.013(1)
C	4*b*	1/2	1/2	1/2				0.015(3)

Table 3
Selected interatomic distances (Å) for $U_6Fe_{16}Si_7$ (A) and $U_6Fe_{16}Si_7C$ (C)

		$U_6Fe_{16}Si_7$ (A)	$U_6Fe_{16}Si_7C$ (C)
U	1 C	–	2.481(1)
	4 Fe(1)	2.786(1)	2.832(1)
	4 Fe(2)	2.899(2)	2.938(1)
	4 Si(1)	2.960(1)	2.981(1)
	4 U	3.548(1)	3.509(1)
	4 U	4.739(2)	4.820(2)
Fe(1)	1 Si(2)	2.460(4)	2.494(2)
	3 Fe(2)	2.564(3)	2.547(1)
	3 Si(1)	2.565(2)	2.569(1)
	3 U	2.786(1)	2.832(1)
	3 Fe(1)	2.841(4)	2.880(1)
Fe(2)	3 Si(1)	2.395(1)	2.410(1)
	3 Fe(2)	2.572(5)	2.514(1)
	3 Fe(1)	2.564(3)	2.547(1)
	3 U	2.899(2)	2.938(1)
Si(1)	4 Fe(2)	2.395(1)	2.410(1)
	4 Fe(1)	2.564(2)	2.569(1)
	4 U	2.960(1)	2.981(1)
Si(2)	8 Fe(1)	2.460(3)	2.494(2)
	6 U	3.351(1)	3.408(1)
C	6 U	–	2.481(1)

respectively, for crystal A, $U_6Fe_{16}Si_7$ and crystal C, $U_6Fe_{16}Si_7C$.

3.3. Crystal structure description

$U_6Fe_{16}Si_7$ and $U_6Fe_{16}Si_7C$ crystallize with the ternary ordered variant of the Th_6Mn_{23} type, commonly referred as $Mg_6Cu_{16}Si_7$ and with a novel "filled" variant of this type of structure, respectively. To the best of our knowledge, $U_6Fe_{16}Si_7C$ is the first example of insertion of carbon in a related Th_6Mn_{23} structure. Numerous compounds adopting the filled Th_6Mn_{23} structure with occupancy of the 4*b* site of the $Fm\bar{3}m$ space group have been reported, the binary compounds $Sc_{11}Ir_4$, $Sc_{11}Os_4$ and $Zr_{11}Os_4$ [16], the ternary compound $Zr_6Zn_{23}Si$ [17] or the so-called *G* phases [18,26]. Other interstitial voids are available in the Th_6Mn_{23} structure [17,27], to accommodate small atoms such as hydrogen, carbon, nitrogen or oxygen. Unlike hydrogen [28,29], our crystallographic refinements of crystals B and C show that carbon or oxygen can only be located on the 4*b* site.

Detailed descriptions of the filled variant of the Th_6Mn_{23}-related structures are available in the literature. They mainly differ by the nature of the coordination polyhedra chosen as building block units. A first model considers individual coordination polyhedra condensing to form large clusters which are fused or are linked by interstitial atoms [16]. A second description presents the structure as composed of 64 polyhedra of two types surrounding atoms located on the 32*f* Wyckoff sites [18]. The crystal structure of $U_6Fe_{16}Si_7C$ is depicted in Fig. 1, which also emphasises the short interatomic contacts. An arbitrary cut off was chosen as the sum of the radii, metallic ones for iron and uranium (r(Fe) = 1.275 Å, r(U) = 1.56 Å) and covalent ones for silicon and carbon (r(Si) = 1.175 Å and r(C) = 0.77 Å). It results in U–Fe(1) distances at 2.832(1) Å, numerous Fe–Fe contacts below 2.547(1) Å and Fe(2)–Si(1) contacts at 2.410(1) Å, leaving Si(2) and C rather isolated. It therefore leads to an original description of the filled Th_6Mn_{23} structure, based on a three-dimensional framework $[U_6Fe_{16}Si_6]$ that defines two octahedral cages centered either by a Si(2) or a C located on the 4*a* or 4*b* sites, respectively (Fig. 1b). The first coordination polyhedra around Si(2) and C are displayed in Fig. 2, they both reside in an octahedron formed by six U atoms, with U–U interatomic distances of 4.820(2) Å and 3.509(1) Å around Si(2) and C, respectively. As seen in Fig. 1b, these octahedra connect by corner-sharing to compose a rock-salt network of octahedral cages within the $[U_6Fe_{16}Si_6]$ framework. Insertion of elements, mainly small atoms such as carbon or oxygen, located in the center of octahedral cages formed by six, 4*f* or 5*f* atoms is well known [30], and has been observed in ternary compounds crystallizing with the Ca_3Ag_8 type of structure as examples [31,32].

The description of the crystal structure of $U_6Fe_{16}Si_7$ is similar to that of $U_6Fe_{16}Si_7C$, except for a major difference that the octahedral uranium motif around the 4*b* site is empty. However, the absence of C directly influences the interatomic distances, peculiarly the short contacts that were emphasized in the previous paragraph. The U–Fe(1)

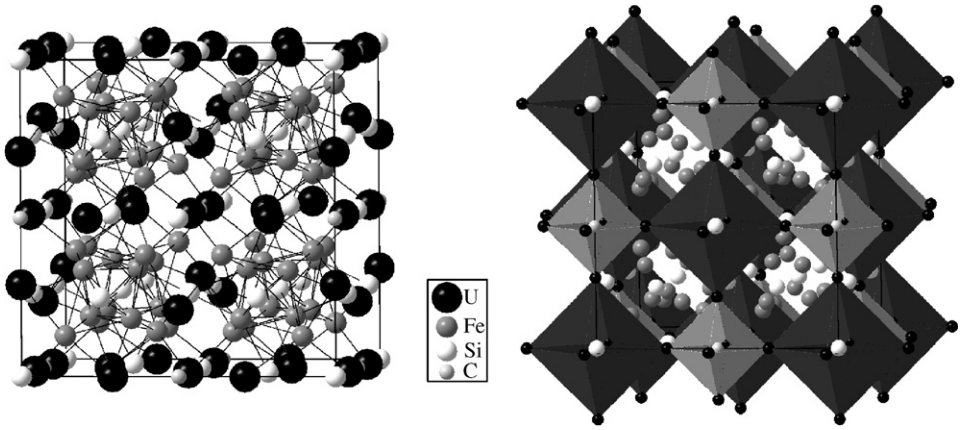

Fig. 1. Perspective view of the crystal structure of $U_6Fe_{16}Si_7C$ along with the short interatomic contacts (a). Polyhedral view of the arrangement of the U6-octahedral motifs, centered by Si2 (dark grey) and C (middle grey) (b).

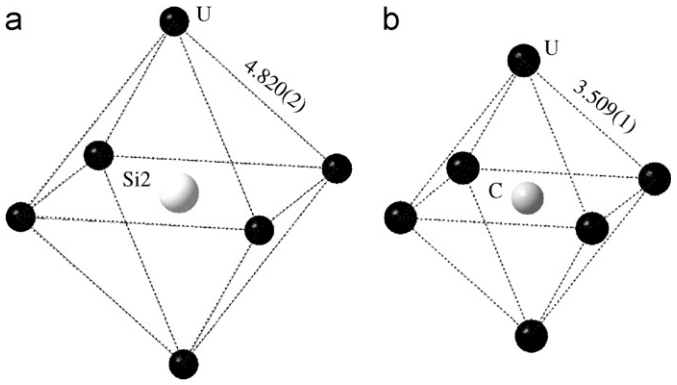

Fig. 2. Coordination polyhedron around Si2 (a) and C (b). The U–U interatomic distances are given in Å.

and Fe(2)–Si(1) distances shrink to 2.786(1) and 2.395(1) Å, respectively, whereas the Fe–Fe contacts expand and no Fe–Fe contacts are shorter than 2.564(3) Å.

3.4. Magnetic properties

Figs. 3 and 4 present the temperature dependence of the magnetic susceptibility $\chi(T)$ of $U_6Fe_{16}Si_7$ and $U_6Fe_{16}Si_7C$ in the temperature range 2–300 K, for an applied field of 5 kOe. The susceptibility of $U_6Fe_{16}Si_7$ remains almost constant over the entire temperature range, with a low value of order 7×10^{-4} emu/mol, featuring a Pauli paramagnetic behavior, which is a direct evidence of the strong hybridization between the 5*f* electrons of U and the 3*d* electrons of Fe. The thermal variation of the susceptibility of $U_6Fe_{16}Si_7C$ gives no evidence of any long-range magnetic ordering in the whole temperature domain. The inverse magnetic susceptibility (inset of Fig. 4) is strongly curvilinear and can be fitted using a modified Curie–Weiss law $\chi = (C/T - \theta_p) + \chi_0$ over the temperature range 100–300 K. In this case, the values of the Curie constant (C), the paramagnetic Weiss temperature (θ_p) and the temperature-independent term (χ_0) are 4.0(2) emu mol^{-1} K, 57(1) K and 5.7(1) $\times 10^{-2}$ emu mol^{-1}. The low value of the

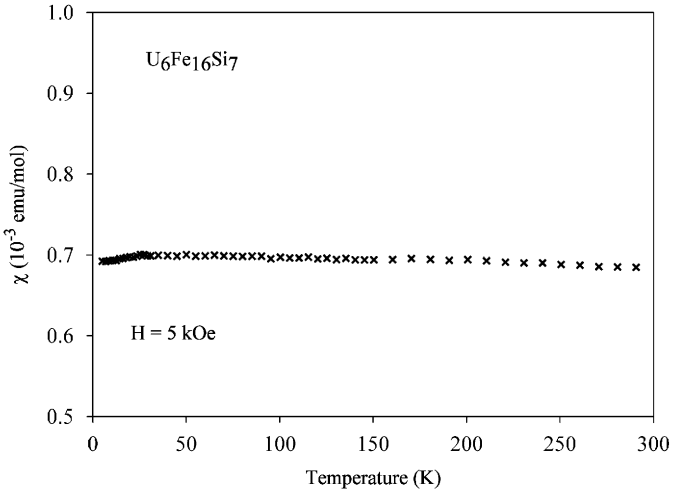

Fig. 3. Temperature dependence of the DC magnetic susceptibility of $U_6Fe_{16}Si_7$ measured under $H = 5$ kOe.

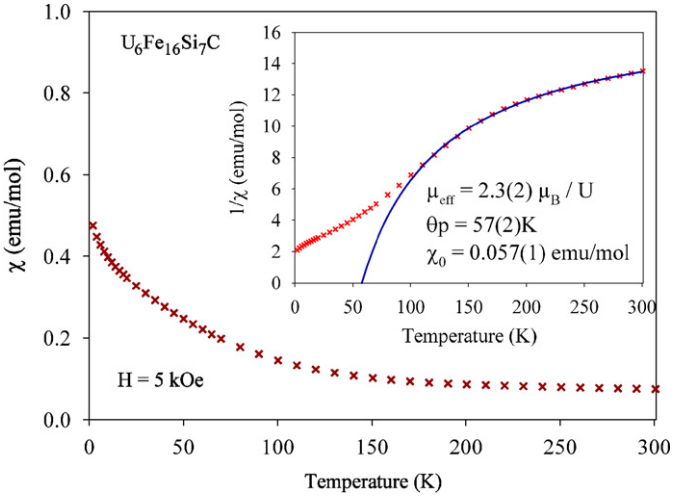

Fig. 4. DC susceptibility of $U_6Fe_{16}Si_7C$ measured in a field of 5 kOe. The inset shows the inverse susceptibility (cross), the solid lines represent the fit of the data according to a modified Curie–Wiess law, for the temperature ranges 100–300 K.

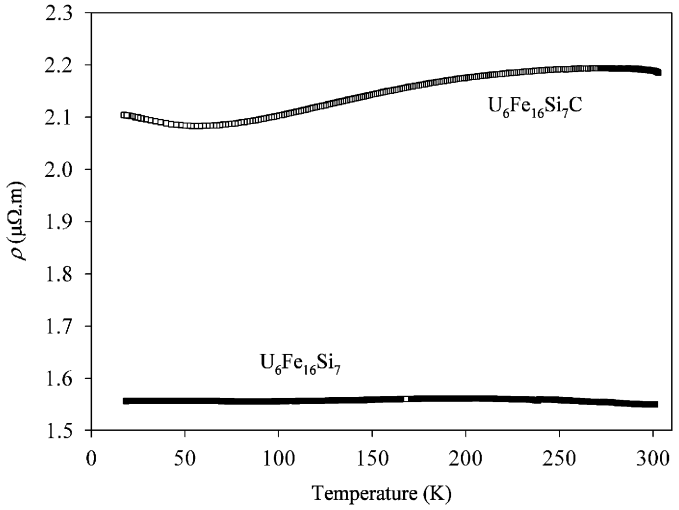

Fig. 5. Temperature dependence of the electrical resistivity of $U_6Fe_{16}Si_7$ and $U_6Fe_{16}Si_7C$.

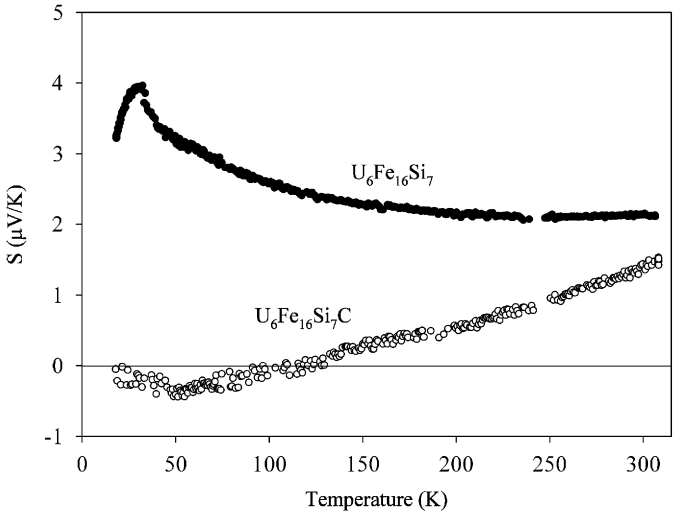

Fig. 6. Temperature dependence of the thermopower of $U_6Fe_{16}Si_7$ and $U_6Fe_{16}Si_7C$.

Curie constant suggests only a contribution to the paramagnetism from the U atoms. The effective paramagnetic moment per U atom estimated at $\mu_{eff} = 2.3(4)\,\mu_B$/U, which compares well with the value obtained for $U_{1.2}Fe_4Si_9$ [8], indicates a substantial reduction of the magnetic moment from the free ion value. Unlike the itinerant behavior of the U-5*f* electrons in $U_6Fe_{16}Si_7$, this implies that the U atoms in $U_6Fe_{16}Si_7C$ may carry some localized electrons in the 5*f* shells. At lower temperature, the significant deviation from the fit may indicate a subsequent reduction of the magnetic moments in $U_6Fe_{16}Si_7C$, pointing out a depopulation of the magnetic ground state, moving the system towards delocalization upon decreasing the temperature (Fig. 4).

3.5. Electrical resistivity and thermoelectric power

The temperature dependence of both the electrical resistivity and the thermoelectric power of $U_6Fe_{16}Si_7$ and $U_6Fe_{16}Si_7C$ are shown in Figs. 5 and 6 for $18 < T < 300$ K, respectively. For both compounds, the measured properties show small values of few μΩm and few μV/K, which compare well with the values of typical metals. However, the linear character of resistivity as a function of the temperature points out that they do not behave as a simple metal. Their electrical resistivity $\rho(T)$ remains almost constant, with a value of 1.55 μΩm and 2.15 μΩm for $U_6Fe_{16}Si_7$ and $U_6Fe_{16}Si_7C$, respectively. Such a behavior is more likely reminiscent of the behavior of semi-metals. In line with the metallic character of the investigated materials, the total change in the Seebeck coefficient is very small (ca. 4 μV/K). The thermopower of $U_6Fe_{16}Si_7$ is about 2 μV/K at room temperature. It increases smoothly as the temperature deceases. A small positive maximum is observed at 30 K, which may be associated with some electronic perturbations such as Kondo scattering. For $U_6Fe_{16}Si_7C$, the thermoelectric power is slightly positive, it linearly decreases with diminishing the temperature down to about 50 K, where $S(T)$ forms a broad negative minima. At lower temperature, the thermopower rises to zero.

Based on the investigated properties, the influence of the insertion of C on the electronic structure is tricky to assess. Doping with carbon increases the electrical resistivity, suggesting either a reduction of the mobility or a decrease of the density of conduction electrons, as suggested by the observed localization of the U-5*f* electrons on the susceptibility measurements.

4. Summary

The new compound $U_6Fe_{16}Si_7$ was found during the systematic investigation of the phase equilibria in the U–Fe–Si ternary system. Microprobe analyses revealed that it is a point compound. The identity of the phase was established unequivocally by single-crystal X-ray diffraction experiments. $U_6Fe_{16}Si_7$ crystallizes in the cubic space group $Fm\bar{3}m$ with lattice parameter $a = 11.7206(5)$ Å, at room temperature. The structural model is fully ordered with a distribution of atoms similar to that found in the $Mg_6Cu_{16}Si_7$ structure type. The crystal structure of $U_6Fe_{16}Si_7$ is built up of two U6 octahedral motifs of different sizes which connect by corner-sharing to compose a rock-salt network. The first U6 octahedral motif has U–U distances of 4.739(2) Å, and is centered by a Si atom. The second one has U–U distances of 3.548(1) Å. It is empty, but can easily accommodate interstitial atoms such as carbon. The novel interstitial carbide $U_6Fe_{16}Si_7C$ was successfully synthesized and its crystal structure unambiguously refined on single crystal. It adopts a quaternary ordered variant of the $Mg_6Cu_{16}Si_7$ type, with C atoms located on the 4*b* site of the $Fm\bar{3}m$ cubic space group. Its

lattice parameter amounts to $a = 11.7814(2)$ Å at room temperature.

Magnetic measurements revealed that $U_6Fe_{16}Si_7$ has a temperature-independent behavior. However, the temperature dependence of its electrical resistivity and thermopower point out that it cannot be classified as a simple metal. The thermal variation of the thermopower may reveal that competing interactions are present at low temperature. The magnetic susceptibility of $U_6Fe_{16}Si_7C$ is best described over the temperature range 100–300 K by using a modified Curie–Weiss law with an effective magnetic per U atom significantly lower than the expected value for a free U^{3+} or U^{4+} ion. Such reduction of the magnetic moment suggests that the *5f* electrons are partially localized. Transport measurements indicate that $U_6Fe_{16}Si_7C$ does not behave as a normal metal.

Acknowledgments

This work was partially supported by the exchange Program GRICES/CNRS 2007-2008. We acknowledge the use made of the Nonius Kappa CCD diffractometer through the Centre de Diffraction X de l'Université de Rennes1 (CDIFX).

References

[1] M.S.S. Brooks, O. Eriksson, B. Johansson, J.J.M. Franse, P.H. Frings, J. Phys. F 18 (1988) L33–L39.
[2] L. Paolasini, G.H. Lander, S.M. Shapiro, R. Caciuffo, B. Lebech, L.-P. Regnault, B. Roessli, J.-M. Fournier, Phys. Rev. B 54 (1996) 7222–7232.
[3] L. Paolasini, G.H. Lander, J. Alloy Compd. 303–304 (2000) 232–238.
[4] A.V. Andreev, D. Nižňansky, Y. Homma, H. Onodera, Y. Shiokawa, I. Satoh, Physica B 369 (2005) 100–103.
[5] W. Suski, A. Baran, T. Mydlarz, Phys. Lett. A 136 (1989) 89–91.
[6] B. Chevalier, T. Berlureau, P. Gravereau, L. Fournes, J. Etourneau, Solid State Commun. 90 (1994) 571–573.
[7] D. Berthebaud, A.P. Gonçalves, O. Tougait, M. Potel, E.B. Lopes, H. Noël, Chem. Mater. 19 (2007) 3441–3447.
[8] S. Noguchi, K. Okuda, M. Abliz, K. Goto, K. Kindo, Y. Haga, E. Yamamoto, Y. Onuki, Physica B 246–247 (1998) 456–459.
[9] D. Kaczorowski, H. Noel, J. Phys.: Condens. Matter. 5 (1993) 9185–9195.
[10] A. V Andreev, F. Honda, V. Sechovsky, M. Divis, N. Izmaylov, O. Chernyavski, Y. Homma, Y. Shiokawa, J. Alloy Compd. 335 (2002) 91–94.
[11] J. B Kusma, H. Nowotny, Monatsh. Chem. 95 (1964) 428–430.
[12] L.G. Aksel'rud, Ya.P. Yarmolyuk, I.V. Rozhdestvenskaya, E.I. Gladyshevskii, Kritallografiya 26 (1988) 103–104.
[13] E. Hickey, B. Chevalier, P. Gravereau, J. Etourneau, J. Magn. Magn. Mater. 90-91 (1990) 501–502.
[14] A. Szytula, M. Slaski, B. Dunlap, Z. Sungaila, A. Umezawa, J. Magn. Magn. Mater. 75 (1988) 71–72.
[15] D. Berthebaud, E.B. Lopes, O. Tougait, A.P. Gonçalves, M. Potel, H. Noël, J. Alloy Compd. 442 (2007) 348–350.
[16] B. Chabot, K. Cenzual, E. Parthé, Acta Crystallogr. Sect. B 36 (1980) 7–11.
[17] X.-A. Chen, W. Jeitschko, M.H. Gerdes, J. Alloy Compd. 234 (1996) 12–18.
[18] A. Grytsiv, J.J. Ding, P. Rogl, F. Weill, B. Chevalier, J. Etourneau, G. André, F. Bourrée, H. Noël, P. Hundegger, G. Wiesinger, Intermetallics 11 (2003) 351–359.
[19] Nonius, In: Collect, Denzo, Scalepack, Sortav. Kappa CCD Program Package, Nonius BV, Delft, The Netherlands, 1998.
[20] R.H. Blessing, Acta Crystallogr. Sect A 51 (1995) 33–38.
[21] A. Altomare, M.C. Burla, M. Camalli, G.L. Cascarano, C. Giacovazzo, A. Guagliardi, A.G.G. Moliterni, G. Polidori, R.J. Spagna, J. Appl. Crystallogr. 32 (1999) 115–119.
[22] G.M. Sheldrick, SHELXS97 and SHELXL97. Program for Structure Solution and Refinement, University of Göttingen, Germany, 1997.
[23] P.M. Chaikin, J.F. Kwak, Rev. Sci. Instrum. 46 (1975) 218–220.
[24] O. Tougait, J. Stêpieň-Damm, V. Zaremba, H. Noël, R. Troc, J. Solid State Chem. 174 (2003) 152–158.
[25] J.N. Chotard, O. Tougait, H. Noël, P. Rogl, A. Zelinskiy, O.I. Bodak, J. Alloy Compd. 407 (2006) 36–43.
[26] A. Grytsiv, X.-Q. Chen, P. Rogl, R. Podloucky, H. Schmidt, G. Giester, V. Pomjakushin, J. Solid State Chem. 180 (2007) 733–741.
[27] I. Jacob, Solid State Commun. 40 (1981) 1015–1018.
[28] M. Commandre, D. Fruchart, A. Roualt, D. Sauvage, C.B. Shoemaker, D.P. Shoemaker, J. Phys. Lett. (Paris) 40 (1979) L636–L639.
[29] K. Hardman, J.J. Rhyne, K. Smith, W.E. Wallace, J. Less Common Met. 74 (1980) 97–102.
[30] E. Warkentin, R. Masse, A. Simon, Z. Anorg. Allg. Chem. 491 (1982) 323–336.
[31] A. Perricone, H. Noël, J. Alloy Compd. 383 (2004) 251–253.
[32] V. Kalihari, S.K. Drar, J. Magn Magn. Mater. 294 (2005) 40–48.